Journal of Power Sources 196 (2011) 4545–4554

Contents lists available at ScienceDirect

Journal of Power Sources

journal homepage: www.elsevier.com/locate/jpowsour

Investigation of aluminosilicate as a solid oxide fuel cell refractory

Paul S. Gentile*, Stephen W. Sofie[1]

Montana State University, Mechanical Engineering Dept., P.O. Box 173800, Bozeman, MT, 59717, USA

ARTICLE INFO

Article history:
Received 25 October 2010
Received in revised form
20 December 2010
Accepted 21 December 2010
Available online 13 January 2011

Keywords:
Aluminosilicate refractory
Silicon poisoning
Solid oxide fuel cell
X-ray photoelectron spectroscopy
Electron microscopy
Energy dispersive X-ray spectroscopy

ABSTRACT

Aluminosilicate represents a potential low cost alternative to alumina for solid oxide fuel cell (SOFC) refractory applications. The objectives of this investigation are to study: (1) changes of aluminosilicate chemistry and morphology under SOFC conditions, (2) deposition of aluminosilicate vapors on yttria stabilized zirconia (YSZ) and nickel, and (3) effects of aluminosilicate vapors on SOFC electrochemical performance. Thermal treatment of aluminosilicate under high temperature SOFC conditions is shown to result in increased mullite concentrations at the surface due to diffusion of silicon from the bulk. Water vapor accelerates the rate of surface diffusion resulting in a more uniform distribution of silicon. The high temperature condensation of volatile gases released from aluminosilicate preferentially deposit on YSZ rather than nickel. Silicon vapor deposited on YSZ consists primarily of aluminum rich clusters enclosed in an amorphous siliceous layer. Increased concentrations of silicon are observed in enlarged grain boundaries indicating separation of YSZ grains by insulating glassy phase. The presence of aluminosilicate powder in the hot zone of a fuel line supplying humidified hydrogen to an SOFC anode impeded peak performance and accelerated degradation. Energy dispersive X-ray spectroscopy detected concentrations of silicon at the interface between the electrolyte and anode interlayer above impurity levels.

Published by Elsevier B.V.

1. Introduction

Aluminosilicate is a potential alternate material for refractory and gas delivery tubing throughout solid oxide fuel cells (SOFCs) due to its high tolerance to thermal shock [1], low thermal conductivity, and relatively low cost. Stationary tubular SOFCs utilizing high purity alumina refractory have been operated at 1000 °C for over 69,000 h with less than 0.1% degradation per 1000 h [2], however the industry standard alumina requires expensive processing of the raw material to remove naturally occurring silicon impurities. The studied aluminosilicate containing silica chemically bonded as mullite (96.3% Al_2O_3, 3.7% $Al_6Si_2O_{13}$) can be freeze cast to a wide variety of shapes for which density can be readily manipulated, minimizing manufacturing wastes and further reducing cost. The introduction of Si is of concern due to the potential for silicon diffusion from the aluminosilicate bulk to the surface where a chemical reaction can occur, volatizing the silicon and transporting it in a gaseous form to the fuel cell. Aluminosilicate components can be exposed to air and fuel streams supplied to the fuel cell; therefore silicon poisoning issues are relevant in both reducing and oxidizing atmospheres. It has been shown that silicon accumulates at the triple phase boundary (TPB) where it creates a glassy silicon oxide phase. [3–5] This glassy phase represents an electronic and ionic insulator [6], retards water [7] and may block active nickel catalytic sites resulting in increased activation polarization and thus degradation. The presence of silicon at the TPB may be due to vapor deposition but also can be due to solid state diffusion of silicon impurities in the SOFC electrolyte or silica based glass seals. [8–10] Regardless of the mechanism of transport, the long duration operational requirements of SOFCs exceeding 40,000 h will likely provide sufficient time for transport related degradation.

Chemical reactions at the gas–solid interface can result in the volatility of harmful silicon vapors from aluminosilicate refractory. It is therefore important to understand the change in the aluminosilicate surface chemistry due to bulk diffusion. Silicon diffusion is very sluggish in silica and aluminosilicates due to the strong covalent bonding within the SiO_4 tetrahedra [11,12]. After reacting aluminosilicate (79.8% SiO_2, 20.2% Al_2O_3) with H_2 gas at temperatures from 1300 to 1500 °C, Tso and Pask [13] observed the formation of an outer surface layer of α-Al_2O_3 void of SiO_2 and an intermediate transition layer with SiO_2 content similar to that of mullite. After reacting 3:2 mullite with H_2 the alumina outer layer void of SiO_2 was again observed. The depletion of SiO_2 may be due to the release of SiO gases (Eq. (1)) in a reducing atmosphere. Mullite was also reported to decompose into corundum (Al_2O_3) and

Abbreviations: EDS, energy dispersive X-ray spectroscopy; FE-SEM, field emission scanning electron microscopy; SOFC, solid oxide fuel cell; TPB, triple phase boundary; XPS, X-ray photoelectron spectroscopy; XRD, X-ray diffraction; YSZ, yttria stabilized zirconia.

* Corresponding author. Tel.: +1 406 579 8981; fax: +1 406 994 6292.
E-mail addresses: paulsgentile@hotmail.com (P.S. Gentile), ssofie@me.montana.edu (S.W. Sofie).
[1] Tel.: +1 406 994 6299; fax: +1 406 994 6292.

0378-7753/$ – see front matter. Published by Elsevier B.V.
doi:10.1016/j.jpowsour.2010.12.106

volatile silicon monoxide (SiO) gas in a carbon monoxide (CO) environment (Eq. (2)), where the rate is governed by diffusion rather than the reaction at the phase boundary. [14,15]

$$Al_6Si_2O_{13}(s) + 2H_2(g) \rightarrow 3Al_2O_3(s) + 2SiO(g) + 2H_2O(g) \quad (1)$$

$$Al_6Si_2O_{13}(s) + 2CO(g) \rightarrow 3Al_2O_3(s) + 2SiO(g) + 2CO_2(g) \quad (2)$$

The volatility of silicon vapors from silica at high temperatures has been studied extensively. [16–25] Recently, thermodynamic equilibrium modeling, thermal gravimetric coupled with evolved gas analysis and Rutherford Backscattering transpiration studies were reported to explore the volatility of silicon vapors from silica, 3:2 mullite and aluminosilicate under SOFC operating conditions. [26,27] It was found that an initial rapid release of silicon vapors was followed by a diffusion limited slower release, indicating that surface residues from manufacturing processes or changes in surface chemistry and morphology are contributing to a decrease in chemical reactivity at the gas-solid interface. The mullite bond ($3Al_2O_3\,2SiO_2$) was shown to offer only a slight improvement in silicon stability over SiO_2 in the presence of water vapor where volatile silicon hydroxide ($Si(OH)_4$) (Eqs. (3) and (4)) and oxy hydroxide (SiO(OH)) (Eqs. (5) and (6)) gases dominate. [22,23,25] In addition to silicon hydroxide, oxy hydroxide and monoxide, volatile silane gases may form in a reducing atmosphere. [27]

$$SiO_2(s) + 2H_2O(g) \rightarrow Si(OH)_4(g) \quad (3)$$

$$Al_6Si_2O_{13}(s) + 4H_2O(g) \rightarrow 3Al_2O_3 + 2Si(OH)_4(g) \quad (4)$$

$$2SiO_2(s) + H_2O(g) \rightarrow 2SiO(OH)(g) + 1/2O_2(g) \quad (5)$$

$$Al_6Si_2O_{13}(s) + H_2O(g) \rightarrow 3Al_2O_3 + 2SiO(OH)(g) + 1/2O_2(g) \quad (6)$$

Some species in vapor form could have little to no effect on SOFC performance if they never condense and deposit which may be likely under 700–1000 °C operation, although it could become an emissions concern if harmful vapors are vented. Singh and Vora [28] showed that silicon can deposit on nickel anode SOFC fibers at 1000 °C in the presence of methane reformation. However, the chemical reformation of methane on the nickel surface may yield an additional mechanism (i.e. low partial pressure of water vapor (Eq. (7)) to promote silicon deposition (Eq. (8)) that may not be present in pre-reformed or hydrocarbon free streams. Silicon monoxide gas has been shown to form an amorphous monoxide when condensing on a cooler surface, followed by a phase transformation to a more stable mixture (Eq. (9)). [15] Silane gases may also deposit at the TPB when exposed to oxygen ions transported across the electrolyte.

$$CH_4 + H_2O \rightarrow CO + 3H_2 \quad (7)$$

$$Si(OH)_4(g) \rightarrow SiO_2(s) + 2H_2O(g) \quad (8)$$

$$2SiO(s) \rightarrow SiO_2(s) + Si(s) \quad (9)$$

The objectives of this investigation are to: (1) study the changes in bulk and surface chemistries of aluminosilicate refractory due to diffusion and gas-solid interface reactions, (2) identify the chemistry and bonding mechanisms of aluminosilicate vapors deposited on yttria stabilized zirconia (YSZ) or nickel, and (3) determine the effects of volatile gases released from aluminosilicate on solid oxide fuel cell performance. While extensive efforts have been made to investigate silica and aluminosilicates for a wide variety of high temperature applications this study is specifically focused on SOFC environments at temperatures between 800 and 1000 °C. For IT-SOFC operating temperatures (600–800 °C) solid state diffusion and volatility of silicon are limited by thermodynamics and kinetics [27], making their observation difficult in experiments truncated to last several orders of magnitude less than 40,000 h. SOFC silicon poisoning experiments were conducted at 800 °C to minimize causes of degradation observed at 1000 °C such as nickel agglomeration [29], degradation of 8 YSZ (8 mol% yttria) electrolyte to 9.5 YSZ [30] and delamination due to variations in thermal expansion coefficient.

2. Experimental material and methods

Three separate experiments were conducted: (1) examination of the changes in aluminosilicate surface morphology and chemistry, (2) evaluation of aluminum and silicon deposition on YSZ and nickel, and (3) silicon poisoning in electrolyte supported SOFCs. A low cost aluminosilicate composition (96.3% Al_2O_3, 3.7% $Al_6Si_2O_{13}$) was utilized for this study and freeze cast prior to sintering to achieve approximately 70% theoretical density. Samples were cut into 14 mm squares, 2 mm thick, from a sintered refractory block utilizing a slow speed diamond saw and air dried for 24 h. Additionally, aluminosilicate powder was crushed from the sintered refractory into a powder utilizing a mortar and pestle (Diamonite™) manufactured from finely powdered synthetic sapphire. Samples were thermally treated in a 6 cm diameter alumina (99% Al_2O_3) tube (McDanel AP35) furnace under controlled flow atmospheres. Gases were fed to a gas control box (Linseis L40/2054) where flow rates were regulated at 1.5 L h^{-1} and 0.7 MPa. The series of gases utilized included humidified ultra-high purity (UHP) air, hydrogen forming gas (5% H_2 Balance N_2), and humidified hydrogen forming gas. A compressed gas cylinder provided the hydrogen forming gas while the UHP hydrocarbon free compressed air was provided with a zero air generator (Packard 2500). The specified gases were humidified utilizing a bubbler containing deionized water at ambient temperature. Complete saturation is assumed based on the gas path length through the water resulting in the partial pressure of water vapor during humidified experiments of $x(H_2O) = 0.027$ atm in air and $x(H_2O) = 0.023$ atm in the reducing hydrogen forming gas. Aluminosilicate square samples under the controlled flow atmospheres were heated from ambient to 1000 °C at a ramp rate of 5 °C min^{-1}, held at temperature for 100 h, cooled to ambient conditions at 5 °C min^{-1} and stored in polyethylene airtight bags at room temperature until analysis. The untreated samples were analyzed as the freeze cast and sintered block prior to any long duration thermal treatment.

The morphology and chemistry of silicon species deposited on nickel oxide and YSZ pucks was studied utilizing nickel oxide (Alfa Aesar Lot #C01R001) and 8 mol % yttria stabilized zirconia (TZ-8YS, Tosoh Corporation) powder separately pressed into pellets (1.27 cm diameter) in a uniaxial press at 35 MPa and 70 MPa, respectively. NiO and YSZ pellets were pressure-less sintered in air at 5 °C min^{-1} from ambient to 1400 °C (NiO) and 1500 °C (YSZ), dwelled at the maximum temperature for 2 h, and cooled back to ambient temperature at 5 °C min^{-1}. Four pellets at a time were then thermally treated in the alumina tube furnace in humidified UHP air, forming gas (5% H_2, balance N_2), or humidified forming gas. Gases were controlled as previously described. One NiO and one YSZ pellet were placed in the furnace in direct physical contact with the aforementioned aluminosilicate powder; two additional pellets (one NiO and one YSZ) were placed 15 cm downstream free of physical contact with the aluminosilicate powder. Both sets of pellets were placed within the hot zone of the furnace, equidistance from the center.

2.1. Characterization

Field emission scanning electron microscopy (FE-SEM), energy dispersive spectroscopy (EDS), X-ray photoelectron spectroscopy (XPS) and X-ray diffraction (XRD) were used to study the change in the bulk (>20 μm below surface), bulk-surface (penetration depth of < 20 μm) and surface (<0.01 μm penetration depth) of alumi-

nosilicate under SOFC operating conditions. FE-SEM (Zeiss VP55 Supra) was used to image the microstructure of the aluminosilicate, bonding of the vapor deposited aluminum and silicon on the YSZ and NiO pucks, and cross sections of SOFC unit cells. Sputter coating using an iridium target at 20 mA for 30 s, carbon tape and graphite paste were used to permit the imaging of the electronically insulating samples. EDS elemental mapping was used to evaluate the dispersion of Si in the sputter coated aluminosilicate, YSZ and NiO samples. Bulk-surface scans show the atomic concentrations with a penetration depth of less than 20 μm, and cross section scans study the bulk. EDS is not a quantitative method but does effectively detect small variations in trace Si concentration as a function of position and can be used for relative comparison. EDS maps, point scans and line scans were conducted with a 20 kV energy beam. XRD (X1-Advanced Diffraction System, Scintag Inc., USA) was utilized to detect the presence of new phases in the aluminosilicate powder after thermal treatment for 100 h at 1000 °C under humidified air, forming gas or humidified forming gas. The XRD tube introduced the X-rays at 45 kV and 40 mA, while the detector was operated at 1 kV. Scans were collected from 2θ angle of 20° to 95° at step increments of 0.05°. Phases were compared against the database of JCPDS powder diffraction files.

XPS, also known as electron spectroscopy for chemical analysis (ESCA), was used to study the changes in surface molecular chemistry of the aluminosilicate, YSZ and NiO samples due to thermal treatments as previously described. All XPS spectra were obtained using a PHI MultiTechnique system (Model 5600). The Electron Energy Analyzer (Model 10-360) incorporated into the 5600 is an SCA, and the input lens to the analyzer is an Omni Focus III lens. All spectra were obtained with the X-ray source operating at 300 watts (15 kV). The excitation X-ray source used was a MgKα monochromator (Model 10-610) located at 54.7° relative to the analyzer axis. The Omni Focus III lens was used to scan the spectrum while the SCA was operated at constant pass energy, resulting in constant resolution across the entire spectrum. All of the spectra were obtained using an 800 μm diameter analysis area and samples were mechanically fastened to the specimen mount. A broad scan survey spectrum was first obtained to identify the elements present and the elemental composition. All XPS spectra recorded and stored using the software system (AugerScan Version 3.22) were taken at a pass energy of 46.95 eV with a step size of 0.400 eV. Since the samples studied were insulating charge compensation was applied. To ensure proper charge correction on the insulating samples the position of the C 1s line from adventitious hydrocarbon was measured. Any shift from 284.8 eV [31], indicative of static charging, was compensated with adjustment of emission control (mA) and electron energy (%). Once the survey scan was completed detailed multiplex scans of the peaks of interest were obtained for a more comprehensive picture of the chemical composition. The narrow scans were adjusted to encompass the peaks and were obtained with pass energy of 23.5 eV and a step size of 0.025 eV. Each scan was swept and cycled repeatedly for averaging. XPS peak intensities of the Al(2p) and Si(2p) spectrums were measured for the aluminosilicate after background signals were subtracted using the Shirley integration method. The background level upon which the peak is superimposed is a characteristic of the specimen, the excitation source and the transmission characteristics of the instrument. Surface Si/Al ratio was calculated using the equation below [32];

$$(\text{Conc. of Si})/(\text{Conc. of Al}) = \left(\frac{I_{\text{Si}}}{I_{\text{Al}}}\right)\left(\frac{\text{ASF}_{\text{Al}}}{\text{ASF}_{\text{Si}}}\right) \quad (10)$$

where I and ASF are the intensity of the spectrum and the atomic sensitivity factor of an individual element, respectively. The ASF of each element for the monochromatic X-ray source utilized at 54.7° are Al(2p) = 0.234 and Si(2p) = 0.339. [31]

2.2. Electrochemical performance test

The electrochemical performance test apparatus utilized has been described in detail elsewhere. [26,33] Commercial grade electrolyte supported button cells (NextCell) with an electrolyte diameter of 25 mm and active area of 1.2 cm^2 were operated at constant voltage (0.7 V) and temperature (800 °C) for over 225 h. The cells were brought from ambient to 800 °C at a rate of 2.5 °C min^{-1} in a clamshell furnace, with N_2 supplied to the anode (50 mL/min) and UHP air to the cathode (50 mL/min). During operation H_2 (99.999%) humidified via a room temperature bubbler to saturation was supplied to the anode (73 mL/min) and UHP air was supplied to the cathode (218 mL/min). The cell was sandwiched between two 6 cm diameter Inconel metal platens which delivered the fuel to the anode (top) and air to the cathode (bottom) through a 0.635 cm hole bored through their center axis. Stacked from the bottom to top platen was silver paste enhancing the electrical connection, silver mesh disc, button cell and nickel foam without contact paste. The sample cell (100610) had 10.5 grams of the aforementioned aluminosilicate powder in the hot zone of the fuel feed line while the reference cell (100625) did not have any aluminosilicate present. Post mortem cross sectional analysis was conducted on fractured cells via FE-SEM and EDS.

3. Results and discussion

3.1. Aluminosilicate surface morphology and chemistry

FE-SEM micrographs with EDS maps overlaid are presented in Fig. 1 for the aluminosilicate samples untreated or after heat treatment for 100 h at 1000 °C in dry reducing gas, humidified reducing gas or humidified air. Micrograph EDS maps of the aluminosilicate show silicon dispersion across the bulk-surface. The aluminosilicate material after treatment in humidified hydrogen or humidified air indicates Si migration is accelerated in the presence of water vapor, yielding a more uniform distribution of Si at the bulk-surface. Surface diffusion occurs along defects and is typically faster than bulk chemical diffusion in silicon systems. [34] EDS maps of the cross section of all the aluminosilicate samples after thermal treatment show the dispersion of Si in the bulk is mainly between alumina clusters. Solid state diffusion of silicon within the aluminosilicate bulk is likely occurring along these grain boundaries. The EDS cross section map of the forming gas sample (Fig. 1 top center) includes the bulk-surface, demonstrating a higher concentration of Si in the bulk-surface compared to the bulk. Uncertainty for EDS concentration analysis is generally ±5% [35] and can only be used for relative comparison rather than to obtain quantitative data. Fig. 2 shows relative Si concentration calculated using EDS is significantly higher at the bulk-surface compared to the bulk for all thermally treated samples, but not the untreated sample. The enrichment of silicon concentrations at the surface is likely due to silicon diffusion rather than alumina volatility since alumina has been demonstrated to be stable in the presence of water vapor up to 1300 °C [36]. Higher relative silicon concentrations at the bulk-surface indicate the rate of silicon solid-state diffusion in the bulk is faster than the rate for which silicon at the bulk-surface is depleted via chemical volatility. The formation of a surface chemistry rich in silicon supplied from the bulk may yield long term steady state silicon volatility rates governed by chemical reactions at the gas-solid interface until the bulk and bulk-surface regions are depleted or a hermetic barrier is formed.

The increase in Si/Al relative concentration ratio from XPS data of the thermally treated samples, Fig. 3, indicates the migration of silicon to the surface from the bulk during thermal treatments. This surface XPS trend is found to be similar to the EDS bulk-surface

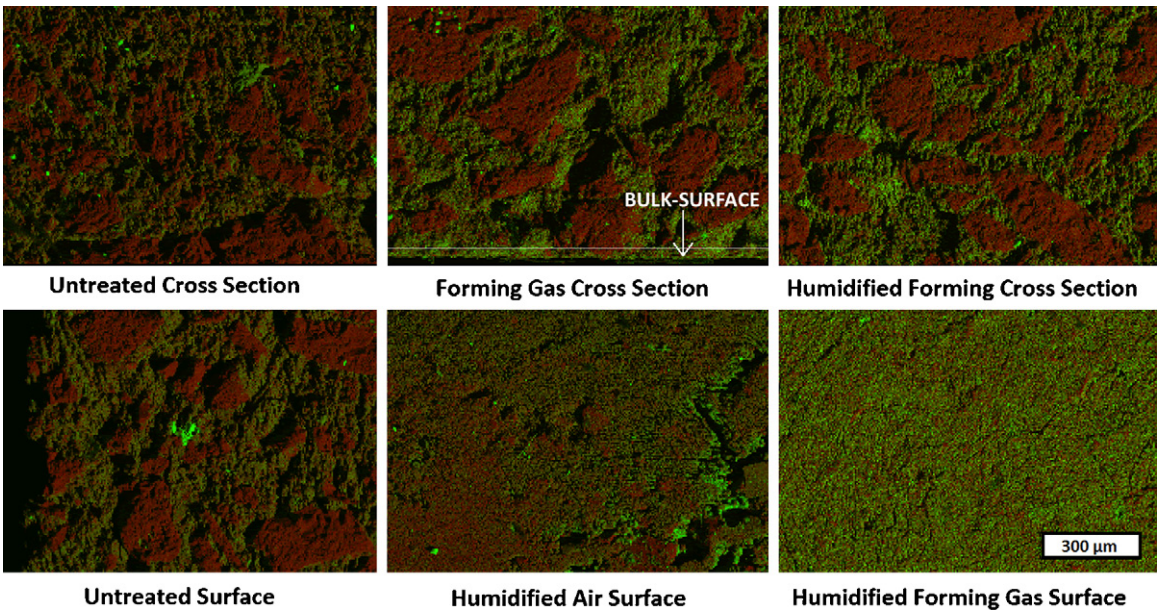

Fig. 1. FE-SEM micrographs with overlaid EDS maps of the cross sections (top row) or bulk-surface (bottom row) of aluminosilicate material untreated or thermally treated at 1000 °C for 100 h in the stated gas. Si is displayed in green (light gray tone) and Al is displayed as red (dark gray tone). (For interpretation of the references to colour in this figure legend, the reader is referred to the web version of the article.)

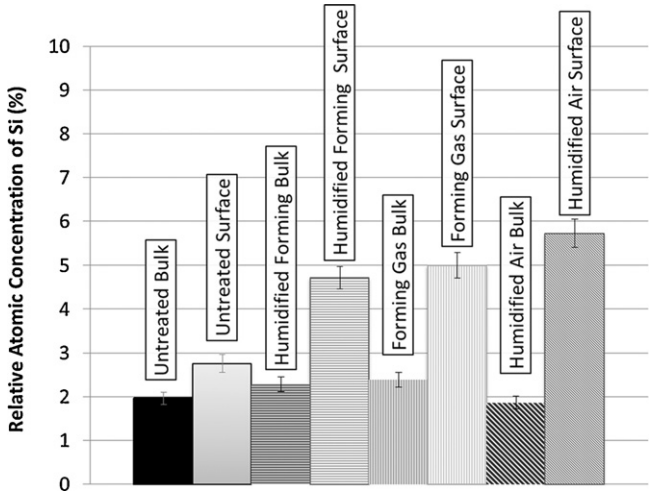

Fig. 2. Qualitative EDS analysis of relative silicon concentration (with error bars) on the cross section or bulk-surface of aluminosilicate specimens treated for 100 h at 1000 °C. All scans were taken at 100× magnification; scan areas are approximately 0.88 mm^2 (1.1 mm × 0.8 mm).

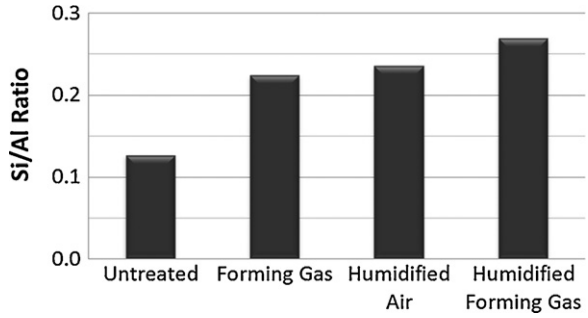

Fig. 3. Relative surface Si/Al concentration ratio calculated via XPS utilizing the Al(2p) and Si(2p) spectrum from aluminosilicate samples untreated or after thermal treatment in the stated gases for 100 h at 1000 °C.

scans. The Al(2p) and Si(2p) peaks for each sample are normalized and superimposed in Fig. 4 to show peak shifts associated with changes in bonding characteristics of Al–Si–O. Variations in the ratio of alumina to aluminosilicate can be correlated with shifts in the Al(2p) and Si(2p) spectrum maxima. [32] Since the dynamics involved in variations of bindings energies are imperfectly understood, we rely on experimental data from standard materials. The range of reported binding energies for several directly comparable aluminum [37–40] and silicon [31,39,41–45] spectra, Table 1, that were carefully evaluated to instrumental calibration and static charge reference values are shown with vertical gray bars in Fig. 4. The Si(2p) peaks show considerably more noise than the Al(2p) due to the low relative concentration of silicon in the refractory utilized in this study. The Al(2p) peak binding energy of the untreated aluminosilicate sample indicates it is composed mainly of alumina near the surface. Thermal treatment resulted in an increase in binding energy of the Al(2p) peak corresponding to increases in the quantity of mullite, in agreement with the EDS results and Si/Al ratio previously discussed. The Si(2p) peaks for the reducing samples indicate a binding energy corresponding to SiO; whereas the untreated and oxidizing heat treated samples show a distribution associated more closely with aluminosilicates. SiO is stable in a reducing atmosphere at 1000 °C, and would remain stable after cool down in the reducing atmosphere to ambient temperatures when the aluminosilicate is exposed to air. The shoulder at the right edge (99.5 eV) of the Si(2p) spectrum is due to the presence of crystalline

Table 1

Compound [references]	Binding energy (eV)	
	Si(2p)	Al(2p)
Si [42,43,31]	99.5	
SiO [41]	101.7	
Al [36,37]		72.8
Al_2O_3 [37–39]		73.7–74.7
Al_2SiO_5, sillimanite [38,40]	102.6	74.6
Al_2SiO_5, kyanite [40]	102.8	74.7
Al_2SiO_5, mullite [40]	103.0	74.8
SiO_2 [44,38]	103.3–103.7	

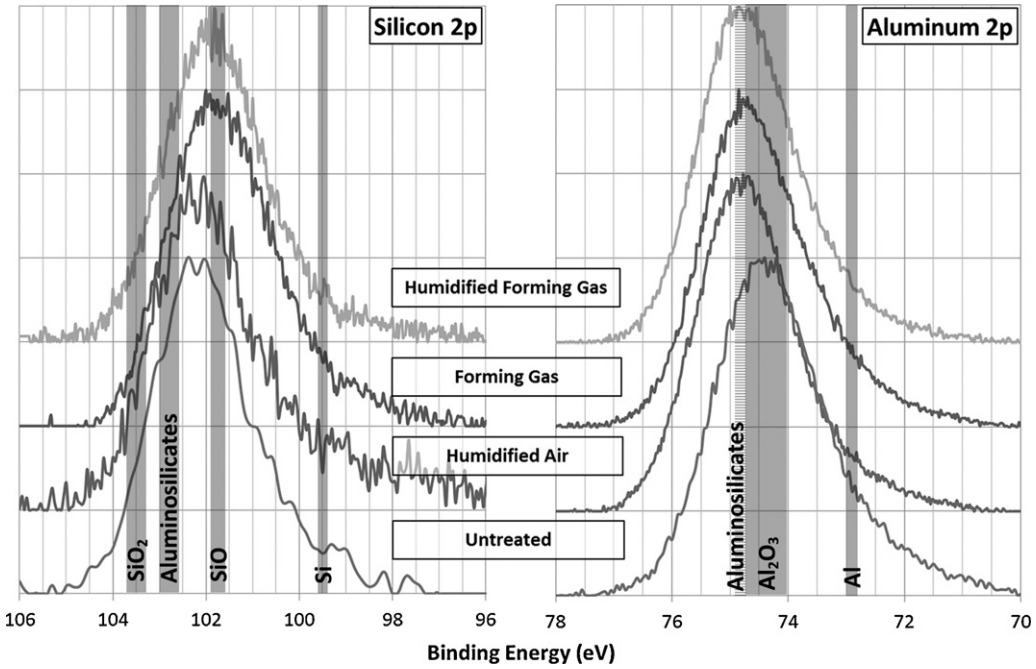

Fig. 4. XPS surface scans of the Si(2p) and Al(2p) spectra from an aluminosilicate samples untreated or after thermal treatment for 100 h at 1000 °C in the stated gases. Gray bars indicate ranges of reported peak maxima (Table 1).

silicon (Si) [42]. This shoulder was previously identified in another aluminosilicate XPS study [32] as the second satellite peak of the Al(2 s) spectrum indicating the presence of extra aluminum oxide. However, the use of a monochromatized X-ray source in this study eliminates these satellite spectra. [46] This is confirmed by the absence of the entire family of minor satellite peaks from the Al(2 s) main spectrum peak located at lower energies (Mg displacement, eV: α_3 – 8.4, α_4 – 10.1, α_5 – 17.6) [31] in all XPS spectrum. Crystalline silicon on the surface of the sample will react with oxygen or hydrogen to form more stable compounds. [27] The depletion of crystalline Si at the surface may be one of several contributing factors leading to the previously reported [27] initial break-in period of rapid silicon release which is followed by slower diffusion limited silicon volatility.

All XRD scans of the aluminosilicate powder untreated or thermally treated include the presence of diffraction peaks at the same 2θ angles, demonstrating no new phases are detected within the limits of XRD. All diffraction peaks were identified and correlated with 3:2 mullite [47] (PDF 15-0776) and alumina [48] (PDF 43-1484) reference diffraction patterns, demonstrating impurity levels are below detection limits. Variations in compound peak intensities related to enrichment of discrete SiO_x phases are indistinguishable or convoluted due to preferred orientation.

3.2. Aluminum and silicon deposition on YSZ and nickel

FE-SEM images with corresponding EDS elemental maps of the YSZ pellets are shown in Fig. 5 to illustrate the interactions of YSZ, Si and Al in the different atmospheres studied. Strong interaction of the aluminum/silicon adsorbate with the YSZ substrate downstream of the aluminosilicate source, as indicated by wetting of the adsorbate, is shown in both fuel and air atmospheres. Conversely, YSZ specimens in direct physical contact with the aluminosilicate powder in the fuel atmospheres (Fig. 6 left) were void of dominant glassy deposits suggesting a stronger affinity towards silicon vapor species. The FE-SEM micrographs and EDS maps in Fig. 5 clearly indicate aluminum rich clusters are entirely enclosed in an amorphous siliceous layer, but also establishes that aluminosilicate is volatizing to the downstream pellet. EDS did not register a signal from the zirconia substrate within the amorphous siliceous region. The YSZ downstream sample treated in humidified forming gas (Fig. 5 bottom row) includes significantly smaller and more evenly dispersed aluminum containing clusters throughout the amorphous siliceous layer in comparison to both YSZ samples treated in humidified air. Tubular silicon deposits are also observed in the top right hand corner of the humidified forming gas EDS/FE-SEM image (Fig. 5 bottom right image) indicating preferential growth. Figs. 5 and 6 (right) reveal extensive grain and grain boundary enlargement around the edge of the clusters due to the amorphous siliceous layer. Furthermore, the EDS line scan in Fig. 6 confirms increases in the Si concentration (marked a, b, c, d or e) correlate with the grain boundaries locations marked correspondingly along the EDS scan arrow, clearly indicating silicon diffusion into the YSZ along grain boundaries, potentially isolating YSZ grains with a glassy phase.

XPS scans of the same samples were conducted using an 800 μm diameter spot size to ensure maximum averaging. Although FE-SEM and EDS maps show migration into the YSZ, Fig. 7 shows that no changes in peak shape or binding energies are apparent in the Zr(3d) and Y(3d) spectra, implying no new compounds are being formed with the YSZ and deposited silicon within detection limits. This confirms that the mechanism of silicon transport occurs through grain boundaries, and while the silicon may not affect the individual grains from a chemical perspective, an insulating grain boundary region can effectively nullify oxygen ion transport. Under a reducing atmosphere Al(2p) peaks from the YSZ samples in direct contact with aluminosilicate are greater in intensity than the downstream samples, suggesting higher concentrations of aluminum. This correlates with the EDS results that show samples in direct contact with the aluminosilicate, which is predominately alumina (96.3% Al_2O_3, 3.7% $Al_6Si_2O_{13}$), have unperturbed chunks physically adsorbed to the surface; where the downstream samples include regions rich in alumina that are encapsulated in an amorphous siliceous based layer adsorbed onto the YSZ and penetrating the grain boundaries. The amorphous layer is likely

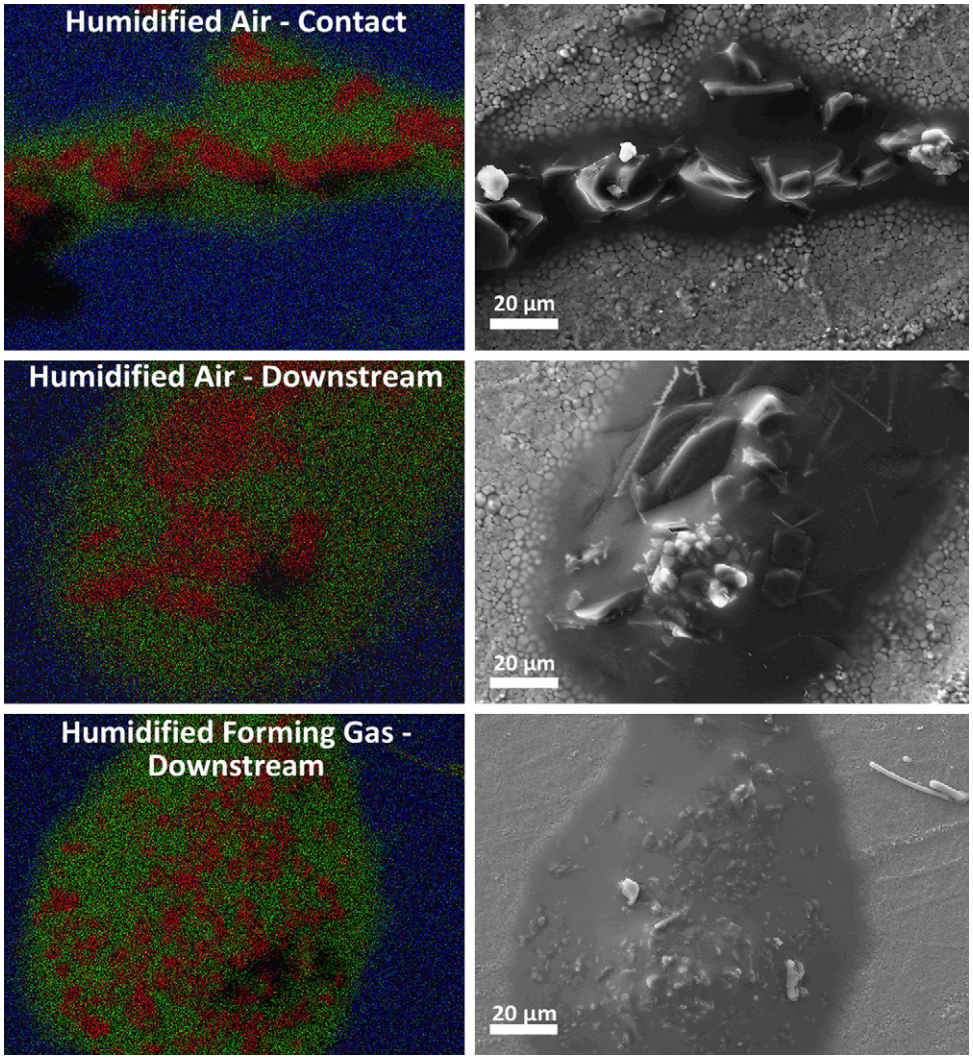

Fig. 5. EDS elemental maps (left) (Si-green (light gray tone), Al – red (mid gray tone), Zr – blue (dark gray tone)) and corresponding FE-SEM micrographs (right) of YSZ pellets in direct physical contact or downstream of the aluminosilicate source at 1000 °C for 100 h in flowing humidified air or humidified forming gas. (For interpretation of the references to colour in this figure legend, the reader is referred to the web version of the article.)

thick enough to inhibit the escape of photoelectrons from the alumina rich under layer, resulting in what appears to be a lower concentration of aluminum. Substantial noise to signal ratio in the Al(2p) spectra from the humidified air samples suggests the siliceous amorphous layer is coherent.

The nickel pellets were all carefully inspected via FE-SEM and EDS for aluminum or silicon bonded to the surface. While small chucks of the aluminosilicate refractory are apparent on the nickel surface no wetting or diffusion of silicon into the nickel grain structure is visually apparent on either the nickel samples in direct

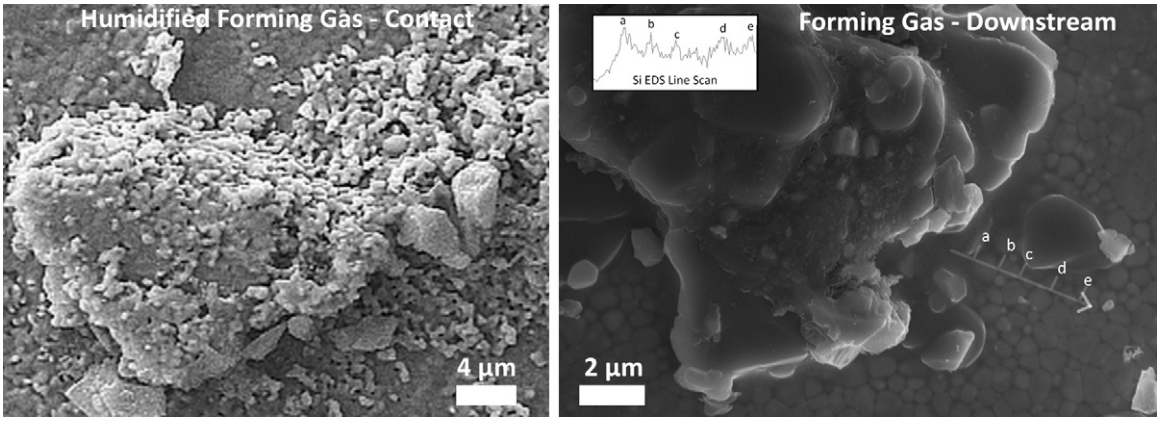

Fig. 6. FE-SEM micrograph and EDS line scan of YSZ pellets in direct physical contact (left) or downstream (right) of aluminosilicate source for 100 h at 1000 °C in the stated gases.

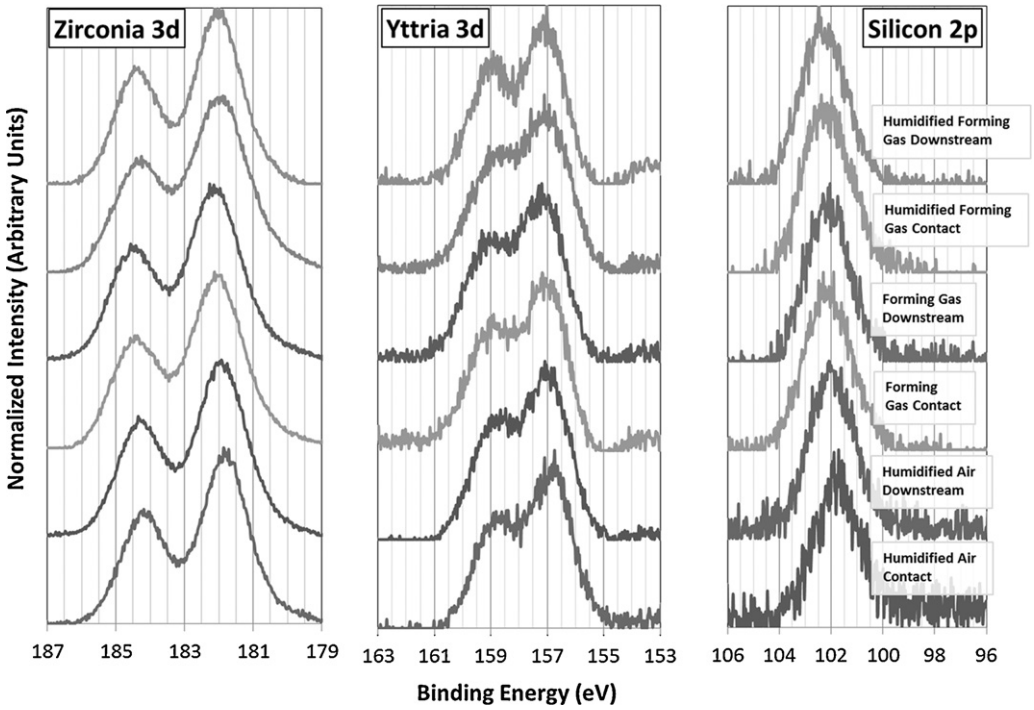

Fig. 7. XPS surface scans of the Zr(3d), Y(3d) and Si(2p) peaks from on YSZ samples in direct physical contact or downstream after thermal treatment for 100 h at 1000 °C in oxidizing and reducing atmospheres.

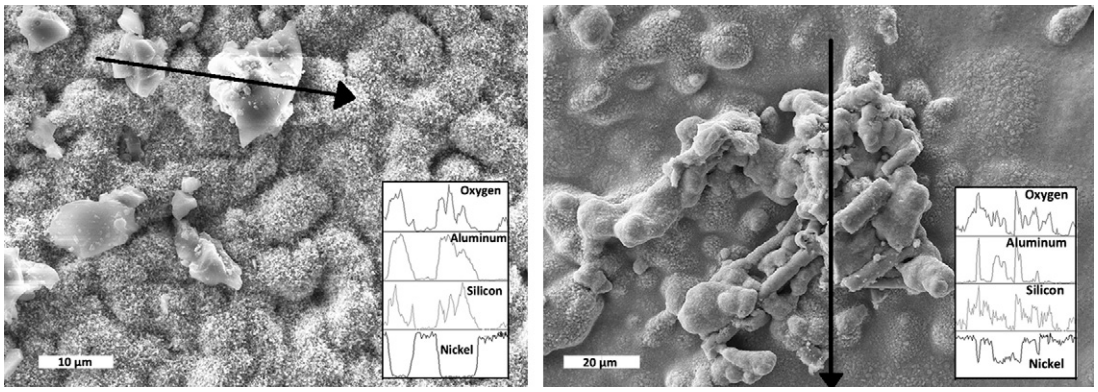

Fig. 8. FE-SEM micrographs and EDS line scans of a nickel pellet in direct physical contact (left) or downstream (right) from aluminosilicate (MSU1) powder for 100 h at 1000 C in flowing humidified forming gas.

physical contact with the aluminosilicate or downstream of the aluminosilicate (Figs. 8 and 9). The nickel sample downstream of the aluminosilicate in flowing humidified forming gas (Fig. 8) had tubular aluminosilicate rods (similar to the YSZ sample thermally treated in the same atmosphere) that appeared physically deposited on the nickel, but were absent of a wetted amorphous siliceous layer. SiO is suggested via thermodynamic equilibrium modeling as a significant volatile silicon gas released from aluminosilicate under a reducing atmospheres at 1000 °C [27]; the observation of aluminosilicate rod shaped deposits only under a humidified reducing atmosphere suggests water vapor encourages preferential growth. Clusters (~20 μm in diameter) on the surface of the nickel pellets after thermal treatment in humidified air include large amounts of refractory impurities (Na, Cl, K, Rh, S, Ca and P) and silicon. Refractory impurities may decrease the activation energy of aluminosilicates, in turn increasing the volatility of silicon containing gases. These impurities appear to have a stronger affinity for the nickel substrate as they were not detected on YSZ pellets.

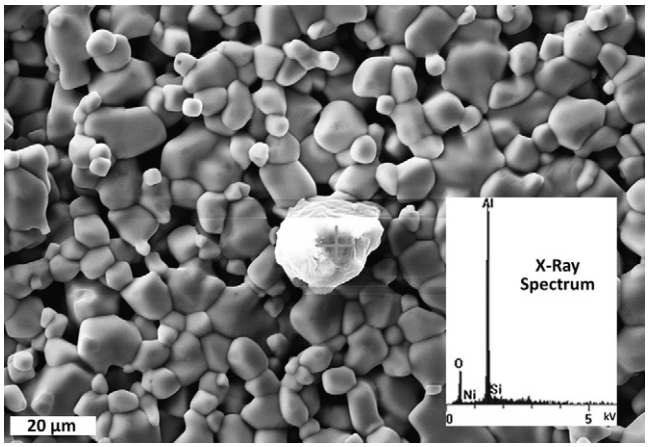

Fig. 9. FE-SEM micrograph and X-ray spectrum (20 kV) of a nickel pellet in direct physical contact with the aluminosilicate source at 1000 °C for 100 h in flowing humidified air.

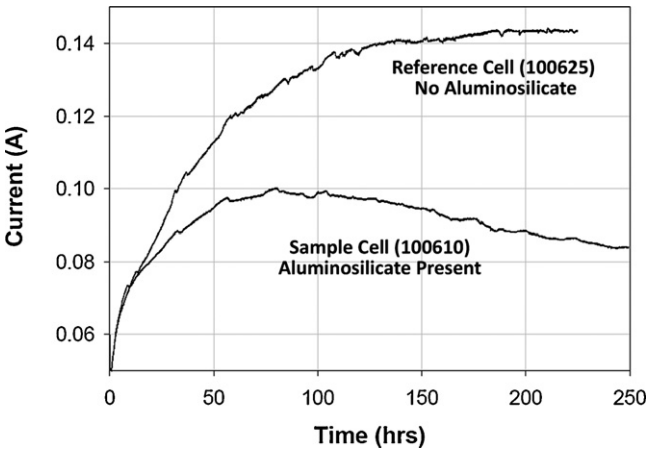

Fig. 10. Electrochemical performance test on two identical electrolyte supported SOFC unit cells (1.23 cm^2 active area) at 800 °C, constant voltage (0.7 V) and flow rates (H_2 – 73 mL/min, UHP air – 218 mL/min). Sample cell (100610) included 10.5 g of aluminosilicate powder in the hot zone of the fuel feed line.

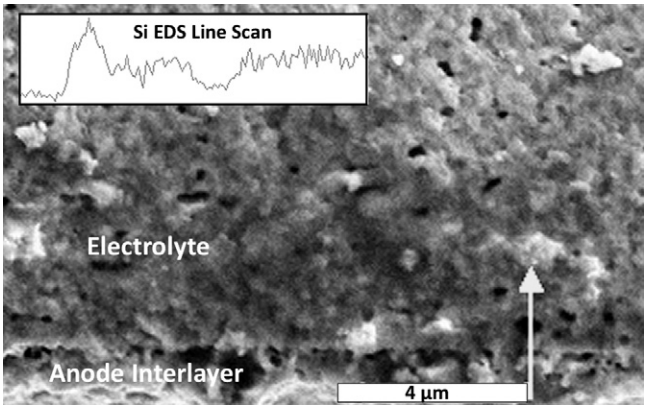

Fig. 11. FE-SEM micrograph and Si EDS line scan of the cross section of the planar SOFC sample cell (100610) after being run for 250 h at 800 °C and constant voltage (0.7 V) with aluminosilicate present in the hot zone of the fuel delivery system. A Si peak is detected at the triple phase boundary; the constant detection level in the electrolyte is presumably YSZ impurity.

The surface of the nickel is visibly different in Fig. 8 compared with Fig. 9 due to the reduction of the nickel oxide pellet to form metallic nickel. EDS line scans (Fig. 8) demonstrate the presence of oxygen correlates with aluminum and silicon yet is absent where nickel is present, indicating the reduction of nickel oxide to metallic nickel during the thermal treatments in the reducing atmospheres is the cause of change in morphology. The change in chemical composition from nickel oxide to nickel metal can result in significantly different interactions and wetting of adsorbate with aluminum and silicon vapor deposits. However, despite the weaker metallic bonding in the reduced nickel samples the formation of an amorphous siliceous phase or silicon adsorption/diffusion into the nickel bulk is not apparent, indicating that silicon poisoning may be more strongly associated with degradation of oxygen ion transport in YSZ electrolytes and anode cermets.

3.3. SOFC silicon poisoning

Results of electrochemical performance testing presented in Fig. 10 on two identical commercial SOFC button cells under duplicate experimental conditions, with the only exception the presence of aluminosilicate in the hot zone of the anode fuel delivery tube, indicate silicon poisoning can occur in relatively short time scales at lower temperatures than the studies above. The reference cell (100625) performed as expected based on the manufacturer's specifications. [49] However, the sample cell (100610) with aluminosilicate present reached 71% of the reference cell peak performance and degraded 15% in 150 h. The reference cell and sample cell followed an identical rate of performance increase during the first 15 h. The initial SOFC break-in period showing substantial performance improvement during startup may be attributed to changes in the electrode microstructural and cathode/electrolyte interface chemistry [50], or activation of the anode through reduction of the nickel oxide to nickel metal and increase of the triple-phase boundary [51]. The reference cell continues to increase current output during cell activation to 0.14 A at 0.7 V until it stabilizes at 150 h. However, the sample cell current output begins to steadily decline at 100 h after reaching a maximum of only 0.10 A at 0.7 V. A previously conducted experiment in our research facility on commercial electrolyte supported SOFCs from an alternate supplier where the aluminosilicate was introduced in situ into the hot zone of the fuel delivery tube demonstrated immediate performance degradation followed by a steady state decline in power output further supporting the silicon induced degradation of these cells is due to the refractory material. [26] The aluminosilicate powder represents a high surface area flow field designed to reduce kinetic limitations and accelerate the volatility of silicon species. Although the high surface area flow field may not be a direct representation of commercial applications for aluminosilicate refractory, the long operating times of stationary SOFCs and extensive use of refractory material provide an ample opportunity for silicon poisoning by vapor species.

Post-mortem cell analysis conducted via FE-SEM and EDS (Fig. 11) on the sample cell revealed silicon within the YSZ electrolyte. A clear distinction in silicon concentration was identified in the anode interlayer compared with the electrolyte suggesting silicon impurities in the YSZ are a significant source. Furthermore, small regions of relatively high concentrations of silicon are observed at the anode/electrolyte interface in the sample cell as seen in the EDS line scan (Fig. 11). At this time we are not able to determine whether the silicon has migrated via solid state diffusion from the anode interlayer and electrolyte, or if it was vapor deposited as condensed volatile gases released from the aluminosilicate. However, the absence of high silicon concentrations at the TPB of the reference cell, poor sample cell performance and rapid degradation in the sample cell compared to the reference cell suggest silicon is indeed being transported from the aluminosilicate powder and deposited in the hot regions of the fuel cell. Additionally, delamination at the TPB (Fig. 12) was prevalent across the sample cell but not the reference cell. The presence of a siliceous glass between the anode interlayer and electrolyte generates the potential for mechanical stresses due to the mismatch of thermal expansion coefficients that can lead to delamination.

The replacement of high purity alumina with aluminosilicate to reduce SOFC costs where the insulation is not isolated from the cells (tubular more so than planar) is shown to substantially increase degradation. This study suggests that aluminosilicates do release SOFC degrading vapors such that, in parallel with stainless steel interconnect studies and chromium volatility, the development of environmental barrier coatings or infusion of different compounds into the aluminosilicate are necessary to lock up the silicon. Further, planar SOFCs commonly employ glass seals which use anywhere from 8 to 53% silica and 5–11% alumina [52,53]. Due to the required physical contact between the glass seal and electrolyte to separate oxidant and fuel gas streams, and the observed rapid diffusion of silicon into the YSZ microstructure along the grain boundaries, solid state diffusion of silicon from the glass seal to the TPB seems very plausible. While reactivity of glass seals with chromia containing interconnects has been addressed [52,54], the volatilization of

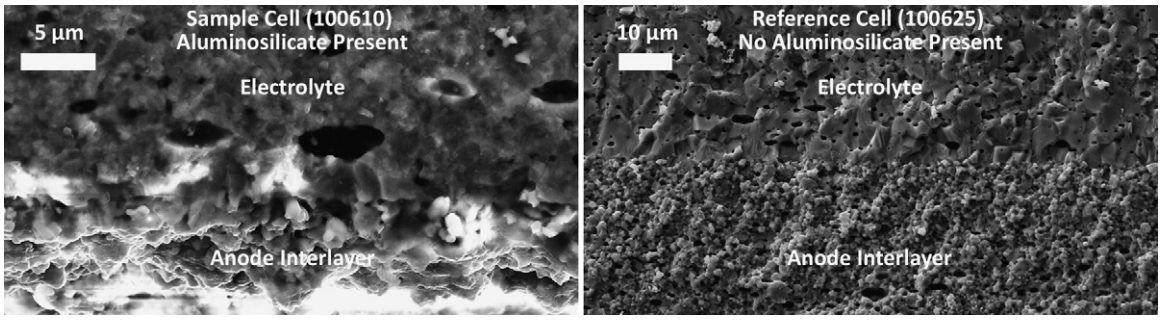

Fig. 12. FE-SEM micrographs illustrating presence and absence of TPB delamination.

silicon from the large class of SiO_2 glass seals and effect on fuel cell performance remains unclear. Individual research studies on this large variety of sealing glasses may be impractical; however, research focused on compositions such as G-18 [55] or other widely used commercial seals may be prudent to study. A calcium borate seal free of silicon [56] or compositional modifiers (V, Ni, Cu, Mn, Ti, Zr, Sr, Ba, Ca, Mg and B) [57] that hold the potential to lockup silica offer opportunity to mitigate concerns of silicon poisoning due to glass seals. Lower temperatures below 800 °C will facilitate kinetic limitations of silicon transport and volatilization, however, the deviation from reference cell performance after only 15 h at 800 °C suggests that transport of silicon to active cell regions will be degrading. Furthermore, silicon's affinity for YSZ observed in the deposition study suggests volatile silicon gases from glass seals may also represent a significant source of long term degradation.

4. Conclusion

It was shown that silicon can diffuse through aluminosilicate refractory bulk to the gas interface, enriching surface mullite concentrations. Surface diffusion is accelerated by water vapor, creating a more uniform distribution of silicon on the aluminosilicate surface. In the absence of hydrocarbon reformation and electrochemical activity, vapors from aluminosilicate were preferentially deposited on yttria stabilized zirconia rather than nickel in both fuel and air atmospheres. Surface adsorption and grain boundary diffusion of siliceous species was detected on the YSZ samples, potentially isolating YSZ grains with a glassy phase; whereas the aluminosilicate was scarcely perturbed upon adsorption to the nickel samples. The presence of aluminosilicate powder within the hot zone of the fuel line supplying the anode caused cell performance to deviate from the reference cell free of aluminosilicate after 15 h at 800 °C, reaching 71% of the maximum power density achieved by the reference cell and degrading 0.1% per hour. Post fuel cell testing identified anode/electrolyte interface delamination and concentrations of silicon above impurity levels in the interface region.

Acknowledgements

The authors gratefully acknowledge Montana State University's Imaging and Chemical Analysis Laboratory; as well as the financial support by the United States Department of Energy, National Energy Technology Laboratory, under SECA Cooperative Agreement No. DE-FC26-05NT42613. Any opinions, findings, conclusions, or recommendations expressed herein are those of the authors and do not necessarily reflect the views of the DOE.

References

[1] K.S. Mazdiyasni, L.M. Brown, J. Am. Ceram. Soc. 55 (Jun 2006) 548–552.
[2] Siemens AG. Siemens.com Global Website October 2010, [Online] http://www.energy.siemens.com/co/en/power-generation/fuel-cells/benefits-features.htm.
[3] M. Aoki, et al., J. Am. Ceram. Soc. 79 (1996) 1169–1180.
[4] S.P.S. Badwal, J. Drennan, A.E. Hughes, B.A.A. Sexton, Mater. Sci. Forum 34–36 (1988) 195–199.
[5] G.M. Ingo, G. Padeletti, Surf. Interface Anal. (1994) 21.
[6] J.L. Hertz, A. Rothschild, H.L. Tuller, J. Electroceram. (September 2007).
[7] M. Mogensen, K.V. Jensen, M.J. Jorgensen, S. Primdahl, Solid State Ionics 150 (2002) 123–129.
[8] M.S. Schmidt, K.V. Hansen, K. Norman, M. Mogensen, Solid State Ionics 179 (2008) 1436–1441.
[9] M. Backhaus-Ricoult, M.F. Tichet, Solid State Ionics 150 (2002) 143–156.
[10] A. Bernasik, K. Kowalski, A. Sadowski, J. Phys. Chem. Solids 63 (2) (2002) 233–239.
[11] P. Borchardt, G. Schmuckerb, M. Schneider, H. Fielitz, Phys. Chem. Chem. Phys. (2003) 2279–2282.
[12] F. Bejina, O. Jaoul, Earth Planet. Sci. Lett. 153 (October) (1997) 229–238.
[13] S.T. Tso, J.A. Pask, J. Am. Ceram. Soc. 65 (8) (1982) 383–387.
[14] V.E. Roshin, A.V. Roshin, A.A. Berdnikov, Y.N. Goikhenberg, Russ. Metall. (Engl. Transl.) 4 (2008) 281–285.
[15] W. Kronert, H. Buhl, Interceram 2 (1978) 140–146.
[16] C.J. van Nieuwenburg, P.M. van Zon, Recl. Trav. Chim. Pays-Bas 54 (1935) p129.
[17] G.W. Morey, J.M. Hesslegesser, Trans. ASME 73 (1951) 865–875.
[18] G.C. Kennedy, Econ. Geol. 46 (1951) 821.
[19] M.D. Allendorf, C.F. Melius, P. Ho, M.R. Zachariah, J. Phys. Chem. 99 (1999) 15284–15293.
[20] E.L. Brady, J. Phys. Chem. 57 (1953) 706–710.
[21] A. Hashimoto, Geochim. Cosmochim. Acta 56 (1992) 511–532.
[22] D.L. Hildenbrand, K.H. Lau, J. Chem. Phys. 101 (7) (1994) 6076–6079.
[23] N. Jacobson, M. Dwight, E. Opila, E. Copland, J. Phys. Chem. Solids 66 (2005) 471–478.
[24] O.H. Krikorian, High Temp. – High Pressures 14 (1982) 387–397.
[25] E.J. Opila, D.S. Fox, N.S. Jacobson, J. Am. Ceram. Soc. 80 (1997) 1009–1012.
[26] P.R. Zafred, S.W. Sofie, P.S. Gentile, Proceedings of the ASME Eight International Fuel Cell Science, Engineering & Technology Conference, Brooklyn, New York, USA, 2010.
[27] P.S. Gentile, S.W. Sofie, C.F. Key, R.J. Smith, J. Am. Ceram. Soc. (2011), in press.
[28] P. Singh, S.D. Vora, A collection of papers presented at the 29th International Conference on Advanced Ceramics and Composites, Cocoa Beach, Florida, January 23–28, 2005, pp. 99–110.
[29] D. Simwonis, F. Tietz, D. Stover, Solid State Ionics 132 (2000) 241–251.
[30] M.S. Sohal, Degradation in Solid Oxide Cells During High Temperature Electrolysis, Idaho National Laboratory, Idaho Falls, Idaho, 2009, INL/EXT-09-15617.
[31] J.F. Moudler, W.F. Stickle, P.E. Sobol, K.D. Bomben, Handbook of X-ray Photoelectron Spectroscopy, Perkin-Elmer Corporation – Physical Electronics Division, Eden Prairie, Minnesota, 1995.
[32] S. Wannaparhun, S. Seal, J. Mater. Chem. 13 (January 2003) 323–327.
[33] A. Lussier, S.W. Sofie, J. Dvorak, Y.U. Idzerda, Int. J. Hydrogen Energy 33 (2008) p945.
[34] Per Kofstad, Truls Norby, Defects and Transport in Crystalline Solids, University of Oslo, Norway, Compendium for the advanced level course Defect Chemistry and Reactions in Solids, (KJM 4120) 2004.
[35] A. Jensen, S.H. Bilde-Sørensen, J.B. Mogensen, M. Hauch, J. Electrochem. Soc. (2007) A619–A626.
[36] E.J. Opila, N.S. Jacobson, D.L. Myers E.H. Copland, Predicting Oxide Stability in High-Temperature Water Vapor, Glenn Research Center, NASA, Cleveland, OH, Research Summary 2006.
[37] L. Ley, F.R. McFeely, S.P. Kowalczyk, J.G. Jenkin, D.A. Shirley, Phys. Rev. 11 (1975) 600.
[38] J. Ashley Taylor, J. Vac. Sci. Technol. 20 (1982) 751–756.
[39] C.D. Wagner, et al., J. Vac. Sci. Technol. 21 (1982) 933–945.
[40] J.C. Klein, D.M. Hercules, J. Catal. 82 (1983) 424–441.
[41] P.R. Anderson, W.E. Swartz Jr., Inorg. Chem. 13 (1974) 2293–2294.
[42] T.P. Nguyen, S. Lefrant, J. Phys.: Condens. Matter 1 (1989) 5197–5204.
[43] V. Atzrodt, T. Wirth, H. Lange, Phys. Status Solidi A 62 (2) (1980) 531–537.
[44] A.F. Povey, R.O. Ansell, T. Dickinson, P.M.A. Sherwood, J. Electroanal. Chem. 87 (1978) 189–201.
[45] M. Klasson, et al., J. Electron Spectrosc. Relat. Phenom. 3 (1974) 427–434.

[46] C.J. Corcoran, H. Tavassol, M.A. Rigsby, P.S. Bagus, A. Weickowski, J. Power Sources 195 (2010) 7856–7879.
[47] A.N. Winchell, H. Winchell, The Microscopical Characters of Artificial Inorganic Solid Substances, Academic Press Inc, New York, 1964.
[48] D. Grier and G. McCarthy, ICDD Granat-in-Aid, 1991, North Dakota State University.
[49] NexTech Materials, AZoM – The A to Z of Materials, October 2010. [Online]. http://www.azom.com/details.asp?ArticleID=2894#_Long_Term_Performance.
[50] E. Ivers-Tiffee, A. Weber, K. Schmid, V. Krebs, Solid State Ionics 174 (2004) 223–232.
[51] G.B. Jung, K.F. Lo, S.H. Chan, J. Solid State Electrochem. 11 (2007) 1435–1440.
[52] P.A. Lessing, J. Mater. Sci. 42 (2007) 3465–3476.
[53] A. Goel, et al., J. Am. Ceram. Soc. 93 (2010) 830–837.
[54] F. Smeacetto, M. Salvo, F.D. D'Herin Bytner, P. Leone, M. Ferraris, J. Eur. Ceram. Soc. 30 (2010) 933–940.
[55] J. Milhans, et al., J. Power Sources 195 (2010) 3631–3635.
[56] T. Zhang, D. Tiang, H. Yang, J. Power Sources 196 (2011) 1321–1323.
[57] S.T. Reis, M.J. Pascual, R.K. Brow, C.S. Ray, T. Zhang, J. Non-Cryst. Solids 356 (2010) 3009–3012.